

# Structural Changes and Coordinatively Unsaturated Metal Atoms on Dehydration of Honeycomb Analogous Microporous Metal–Organic Frameworks

Pascal D. C. Dietzel,<sup>\*,[a, b]</sup> Rune E. Johnsen,<sup>[c]</sup> Richard Blom,<sup>[a]</sup> and Helmer Fjellvåg<sup>[b]</sup>

**Abstract:** Porous metal–organic framework compounds with coordinatively unsaturated metal sites on the inner surface of the pores promise to be valuable adsorbents and catalyst systems, either in industrial applications or as model systems to study interactions with guest molecules. The dehydration process of two isostructural microporous coordination polymers,  $[M_2(\text{dhtp})(\text{H}_2\text{O})_2] \cdot 8\text{H}_2\text{O}$ , termed CPO-27-M ( $M = \text{Co}, \text{Zn}$ ;  $\text{H}_4\text{dhtp} = 2,5$ -dihydroxyterephthalic acid) was investigated by in situ variable temperature X-ray diffraction. Both compounds contain accessible coordination sites at the metal after complete removal of the solvent.

However, despite the analogy of their crystal structures, they behave differently during dehydration. For CPO-27-Co, water desorption is a smooth topotactic process of second order with no concomitant space group change and no increase in microstrain, which is beneficial for the applicability of the material. Removal of the water propagates from the center of the channels outwards. The coordinating water mol-

ecule at the metal desorbs only when almost all the bulk water in the pores has disappeared. In contrast, discontinuities in the powder pattern of CPO-27-Zn indicate the occurrence of first-order transitions. The crystal structures of four of the five individual phases could be determined. The structure of the intermediate phase occurring just before the framework is completely evacuated was elusive in respect to full structure solution and refinement, but it is most probably related to the removal of the axis of threefold symmetry. The zinc-based material experiences a significant amount of strain.

**Keywords:** coordination polymers • microporous materials • single-site catalyst • topotactic transformation • X-ray diffraction

## Introduction


Inorganic–organic hybrid materials that exhibit permanent porosity promise to impact a range of applications, most no-

tably catalysis and gas storage or separation.<sup>[1–6]</sup> Metal–organic frameworks with extremely high apparent surface areas and pore volumes appear as candidates to incorporate coordinatively unsaturated metal sites into porous frameworks.<sup>[7]</sup> Besides being potentially active in catalysis, such accessible metal sites may enhance the interaction of adsorbed gases with the framework and thus increase its utility as a gas storage medium.<sup>[8–16]</sup> The behavior of such a material upon desolvation is crucial for its suitability for application.<sup>[17,18]</sup> Sufficiently robust coordination polymer frameworks will remain stable and show permanent porosity upon solvent removal. In addition to the extremes of collapse or rigid conservation of the long-range order of the framework upon guest removal, more extraordinary accommodation of framework structure to solvent loss have been observed, for example, exceptionally large breathing<sup>[19,20]</sup> or more complex single-crystal-to-single-crystal transformations.<sup>[21–26]</sup> The structures of empty robust frameworks have been investigated in some cases by single-crystal structural analysis.<sup>[27–43]</sup> If the metal atom in the framework is bonded to a solvent molecule, the framework will try to accommodate its remov-

[a] Dr. P. D. C. Dietzel, Dr. R. Blom  
SINTEF Materials and Chemistry  
Department of Hydrocarbon Process Chemistry  
P.O. Box 124 Blindern, 0314 Oslo (Norway)  
Fax: (+47) 220-67-350  
E-mail: pascal.dietzel@sintef.no

[b] Dr. P. D. C. Dietzel, Prof. H. Fjellvåg  
Centre of Materials Science and Nanotechnology  
Department of Chemistry, University of Oslo  
P.O. Box 1033 Blindern, 0315 Oslo (Norway)

[c] R. E. Johnsen  
Department of Chemistry, University of Oslo  
P.O. Box 1033 Blindern, 0315 Oslo (Norway)

 Supporting information for this article contains an animation of the dehydration of CPO-27-Co and additional tables and figures. This information is available on the WWW under <http://www.chemeurj.org/> or from the author.

al. As a result, the framework can collapse and become a) amorphous, or a rearrangement of the coordination environment of the metal can occur, for example, a change in coordination number and/or geometry<sup>[44–46]</sup> or substitution of the former solvent molecule with a less volatile ligand.<sup>[47]</sup> However, if the framework is sufficiently rigid to prevent the previous possibilities, an empty coordination site at the metal forms. Examples of structure determinations of desolvated framework compounds that contain such coordinatively unsaturated metal atoms, also referred to as open metal sites, are rare.<sup>[9,48,49]</sup>

Recently, we reported the compounds  $[M_2(\text{dhtp})(\text{H}_2\text{O})_2] \cdot 8\text{H}_2\text{O}$ , henceforth termed CPO-27-M ( $M = \text{Co}, \text{Ni}$ ),<sup>[9,49]</sup> and Rosi et al. reported the zinc-based metal–organic framework compound MOF-74.<sup>[50]</sup> All of these contain the same microporous honeycomb analogous framework, which contains solvent molecules coordinating the metal. For the nickel and cobalt compounds, we have previously determined the crystal structures of the dehydrated frameworks and shown that the metal is accessible from the evacuated pores after removal of the solvent.<sup>[9,49]</sup> Herein, we present an investigation into the dynamics of the dehydration process for the cobalt and the zinc compounds by in situ powder diffraction using synchrotron radiation with the intention of gaining a better understanding of the sorption process. We observe major differences in the dehydration of the two isostructural frameworks. The high time resolution of the experimental approach enabled us to monitor and elucidate these fast and dynamic structural changes. Our results show how the solvent desorption proceeds in stages, observable by means of X-ray diffraction, and ultimately leads to coordinatively unsaturated metal sites in the fully evacuated frameworks.

## Results and Discussion

For the purpose of straightforward comparability, the compound  $[\text{Zn}_2(\text{dhtp})(\text{H}_2\text{O})_2] \cdot 8\text{H}_2\text{O}$ , CPO-27-Zn, was synthesized, which aside from the varying metal has the same composition as CPO-27-Co and CPO-27-Ni. It differs from MOF-74 in the type of solvent included in the pores. The crystal structure of the as-synthesized material at room temperature and in a dehydrated state at 100 and 150 °C was determined by in situ single-crystal diffractometry (Figure 1). The room temperature structural determinations confirm that CPO-27-Zn is isostructural to CPO-27-Co and CPO-27-Ni. The crystal structure resembles a honeycomb. The intersections of the honeycomb are formed by one-dimensional helical chains of *cis*-edge-connected metal–oxygen coordination octahedra. Adjacent chains are linked by the organic ligand forming the honeycomb, the channels of which have an effective diameter of approximately 11 Å. The inversion centre present in the organic linker results in opposite handedness of the neighboring metal–oxygen chains. In the solvated state, the metal atom is coordinated by one water molecule, with the remaining coordination sites being occu-

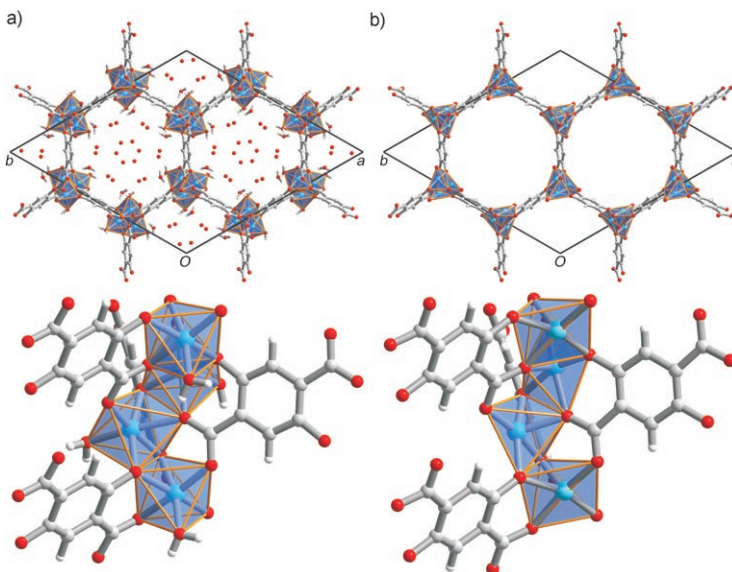


Figure 1. a) Unit cell of the crystal structure of the hydrated CPO-27-Zn (CPO-27-Co is isostructural) along [001] showing the honeycomb topology and one-dimensional solvent-filled channels (top). Threefold helical chain of *cis*-edge-connected metal–oxygen octahedra in the hydrated structure (bottom). b) Unit cell of the crystal structure of the dehydrated framework at 150 °C along [001] (top) and square pyramidal coordination of the zinc cation in the chains with an unoccupied sixth coordination site pointing towards the cavity (bottom).

ried by oxygen atoms belonging to the organic linker. The solutions of the structure at 100 and 150 °C confirm the presence of a coordinatively unsaturated metal site in the dehydrated structure in analogy to CPO-27-Co and CPO-27-Ni. Aside from the loss of one coordinating group, the most pronounced change in the local environment of the zinc atom is the zinc–oxygen bond distance in the position *anti* to the water coordination site, which decreases from 2.273(2) Å at room temperature to 2.128(14) Å at 100 °C and further to 2.086(15) Å at 150 °C, while the remaining four Zn–O distances which are in the range 2.03–2.10 Å at room temperature decrease only little upon dehydration (Table 1).

The time required for the collection of single-crystal diffraction data for these materials (more than a day for a complete hemisphere by using a diffractometer with an X-ray tube) has a significant impact on the accuracy of how well the crystal structure actually reflects the dehydration process the compounds undergo. For instance, when doing the in situ single-crystal study of the cobalt compound in a stream of nitrogen, there was already no remaining water in the structure at 70 °C, even though the TG curve (Figure S5 in the Supporting Information) indicates otherwise. The difference lies mainly in the heating rate which was low for the single-crystal diffraction experiment to minimize thermal stress on the crystal but apparently simultaneously allowed for the removal of all the water in the dry and hot gas stream at comparatively low temperatures. The method is, therefore, unsuitable to monitor faster changes that happen in the course of dehydration. Consequently, techniques of-

Table 1. Comparison of selected bond lengths [ $\text{\AA}$ ] and angles [ $^\circ$ ] for the single-crystal structure determinations of CPO-27-Zn and CPO-27-Co and their respective dehydrated structures (data for CPO-27-Co from ref. [49]).

Bond length or angle	CPO-27-Zn	CPO-27-Zn-373 K	CPO-27-Zn-423 K	CPO-27-Co	CPO-27-Co-368 K
M–O(carboxylate)	2.035(2)	1.987(14)	2.004(13),	2.036(5)	1.997(5),
	2.098(2)	2.089(16)	2.075(14)	2.061(5)	2.067(5)
	2.273(2)	2.128(14)	2.086(15)	2.190(5)	2.078(5)
M–O(hydroxo)	2.042(2)	1.958(13),	1.974(12)	2.041(5)	1.989(5),
	2.058(2)	1.988(12)	1.999(12)	2.048(5)	2.022(5)
M–O(water)	2.119(3)			2.158(7)	
O(hydroxo)-M-O(carboxylate) chelating	84.00(9)	81.3(5)	81.3(5)	84.3(2)	81.8(2)
O(hydroxo)-M-O(carboxylate) nonchelating	80.08(10)	79.3(6)	78.5(6)	81.5(2)	80.8(2)
	84.01(9)	81.0(6)	78.8(6)	84.6(2)	81.3(2)
	85.78(9)	95.6(6)	97.6(6)	89.0(2)	96.8(2)
	94.53(10)	98.6(6)	99.7(5)	95.1(2)	97.1(2)
	96.01(10)	99.3(5)	100.0(6)	95.3(2)	99.9(2)
O(carboxylate)-M-O(carboxylate)	77.22(3)	82.5(2)	82.6(2)	79.65(6)	83.25(7)
	96.11(10)	108.8(7)	107.8(6)	95.2(2)	101.1(2)
O(water)-M-O(carboxylate)	95.00(13)			92.5(2)	
O(water)-M-O(hydroxo)	91.72(13)			92.7(3)	
	95.37(13)			93.0(3)	
	96.75(12)			95.1(3)	

fering a higher time resolution must be used. Real-time synchrotron X-ray powder diffraction experiments have been used to follow the dehydration of zeolite materials.<sup>[51–58]</sup> We, therefore, performed variable-temperature X-ray powder diffraction experiments on beam-line BM01A at the ESRF. The experimental setup permitted the collection of one powder pattern every 107 seconds of which 80% are needed for read-out of the image plate. The remaining 20 seconds are the actual time during which the pattern is recorded. With a heating rate of  $2^\circ\text{Cmin}^{-1}$  below  $200^\circ\text{C}$ , a precise snap-shot of the state of substance under the momentarily prevailing conditions was obtained. Rietveld analysis of the individual scans, therefore, afforded a detailed investigation of the structural changes during dehydration.

The cobalt compound CPO-27-Co exhibits good crystallinity until it is decomposed above  $500^\circ\text{C}$  (Figure 2a; note that the thermal stability is exaggerated by the comparatively slow decomposition kinetics in regard to the heating rate of the synchrotron experiment; the home

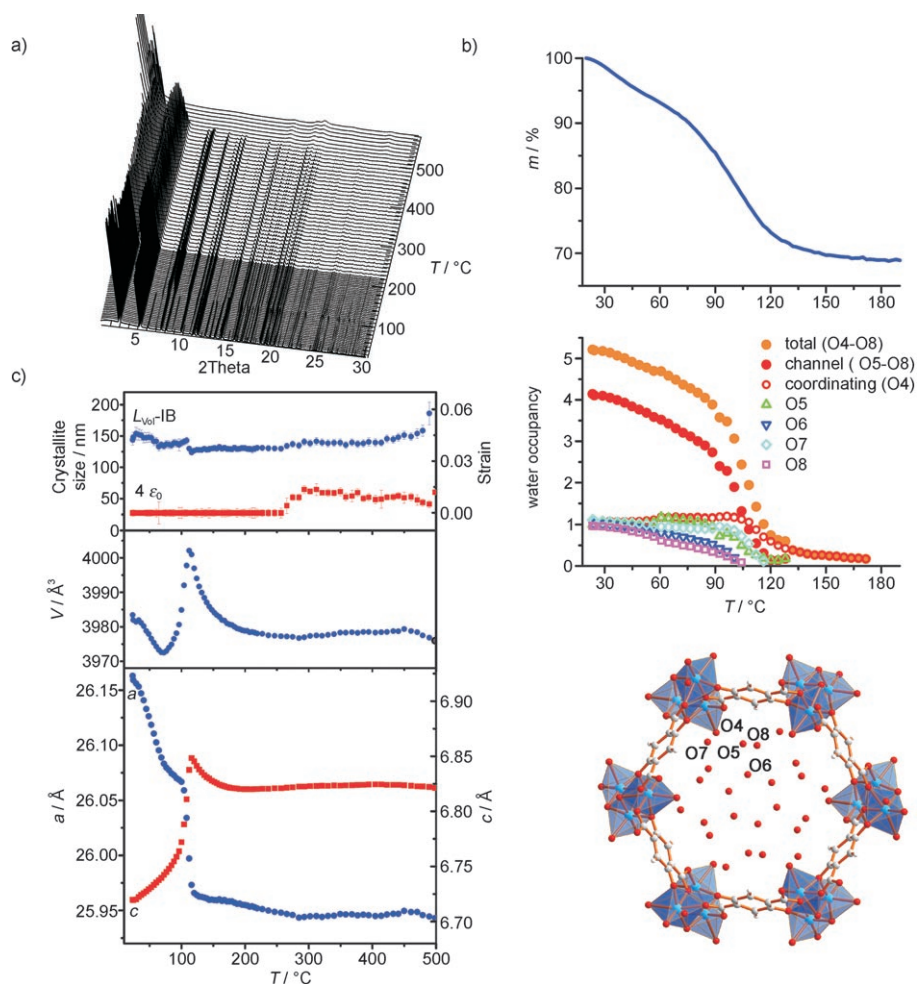


Figure 2. a) Variable temperature X-ray powder pattern of CPO-27-Co; b) site occupancy factor of the bulk and coordinating water molecules plotted against temperature (middle; bottom: visual representation of the numbering scheme; top: weight loss from thermogravimetric experiment with identical heating rate for comparison). c) Analysis of lattice parameters, cell volume, and crystallite size and strain (bottom, standard deviation bars are smaller than symbols except when visible).

lab data with lower heating rates indicate disappearance of crystallinity below 300 °C which is more in congruence with the TG data that shows weight loss related to framework decomposition above 320 °C). The space group of the hydrated and dehydrated crystal structure is identical, and the smooth and continuous change of reflection positions and intensities clearly indicate that the transformation is of second order and topotactic. The most profound changes in reflection positions and intensities occur in the range up to 140 °C, during which almost all of the water leaves the structure, and especially in the temperature range between 100 and 140 °C, in which some reflections almost completely disappear while others significantly increase in intensity reflecting the pronounced changes occurring in the structure. Once the compound is fully dehydrated, the diffraction patterns change very little until the reflection intensities are affected above 450 °C by the onset of decomposition of the framework.

Notably, there is a clear cut difference in how the site occupancy of the individual water positions develops during the dehydration process (Figure 2b). While two of the water molecules (O6 and O8), with O6 the closest to the center of the channel, immediately upon commencement of the experiment continuously diminish in occupancy, the other two bulk water molecules (O5 and O7) leave the structure only to a very small degree below 90 °C, above which their rate of removal increases until all the bulk water has disappeared at  $\approx 120$  °C. The coordinating water molecule (O4) is unaffected until the temperature has reached 108 °C, when already more than three quarters of the bulk water have left the channels. Only then does O4 start to be removed from the structure. Very little of it remains at 140 °C, and the dehydration is complete at 180 °C. The thermogravimetric analysis performed with the same heating rate (Figure 2b) agrees well with the evolution of the site occupancies of the water, thus supporting the validity of this analysis. While the TG curve does not contain any well-developed steps, though, the X-ray analysis reveals that the dehydration consists of overlapping stages in which the removal of the water molecules propagates in general from the center of the channels towards the channel walls, with the extreme being the metal-coordinating water molecule which is most strongly bound and consequently removed last (see the animation which is included in the Supporting Information for a visual presentation of the process).

The variation in unit-cell parameters of CPO-27-Co is closely related to the water content. The *a* parameter decreases and the *c* axis increases when the bulk water content in the channels diminishes (Figure 2c). The changes are most pronounced in the range from 100–120 °C, when the coordinating water starts to depart its position. This leads to a fast contraction of the *a* axis and an increased expansion of the *c* axis. The framework structure itself remains unaffected during the dehydration except for minor adjustments related to the changed unit-cell dimensions and the absence of the coordinating water. Overall, the lattice parameters do not change by a very large amount in relation to their abso-

lute values. The anisotropy of the change can be rationalized in that the evacuation of the contents of the channels is accommodated by a contraction of the *a* axis in an attempt to minimize the empty space, which is only possible to a small degree due to the relative rigidity of the framework, and in turn leads to a stretching of the chains along the *c* axis, similar to an accordion. Note also how the latter is reflected by tilting of the lamellar arranged phenyl rings of the organic ligand in respect to the *c* axis upon removal of the water (best observed in the animation, which is included in the Supporting Information).

It is worthwhile to note that there is no significant micro-strain-induced during the entire dehydration. The material is, therefore, expected to be able to withstand repeated adsorption–desorption cycles without degradation of structural integrity. Only above  $\approx 260$  °C does the strain increase. This temperature coincides with the onset of structural degradation in the corresponding thermodiffraction experiment in the home lab with a slower heating rate (Figure S4 in the Supporting Information). It corresponds, furthermore, with the results of the thermogravimetric experiment, which shows the onset of decomposition at 320 °C (Figure S5 in the Supporting Information).

The variable temperature X-ray powder patterns of CPO-27-Ni<sup>[9]</sup> and CPO-27-Co look very much alike, which indicates that the dehydration proceeds in all likelihood analogously for these two compounds. In contrast, the zinc compound, CPO-27-Zn, differs noticeably from its cobalt homologue in its dehydration behavior. The thermodiffraction (Figure 3a) contains abrupt changes instead of the continuous progression of the patterns as observed for CPO-27-Co. In total, there are five phases in the thermodiffraction. The initial phase 1 is present until 88 °C. It is characterized by a smooth shift in unit-cell parameters. Then, at 92 °C, the reflection positions change discontinuously which results in a modest increase of the *a* axis and a larger contraction of 6.5% of the *c* axis. This phase 2 is present until 104 °C, when phase 3 appears with a diffraction pattern already resembling that of the final high-temperature phase 5. However, before phase 5 appears, the powder patterns degrade in the temperature range of 112–164 °C when the intensity of the reflections pass through a minimum and peak broadening increases to the extent that the higher angle reflections are close to being merged with the background. The two strong reflections of the initial phase acquire additional shoulders on each side. These disappear on further heating, and from 172 °C on the pattern is again well-resolved and stays basically unchanged until 386–488 °C when degradation of the long-range order occurs.

The results of the structure refinement reveal that the trend of occupancy of the bulk water (Figure S12 in the Supporting Information) and changes in unit-cell parameters (Figure 3b) in phase 1 are similar to the cobalt compound. Likewise, the framework structure remains essentially unchanged in this phase. However, the significant changes in lattice parameters on transition to the second phase are naturally also reflected in more pronounced structural changes



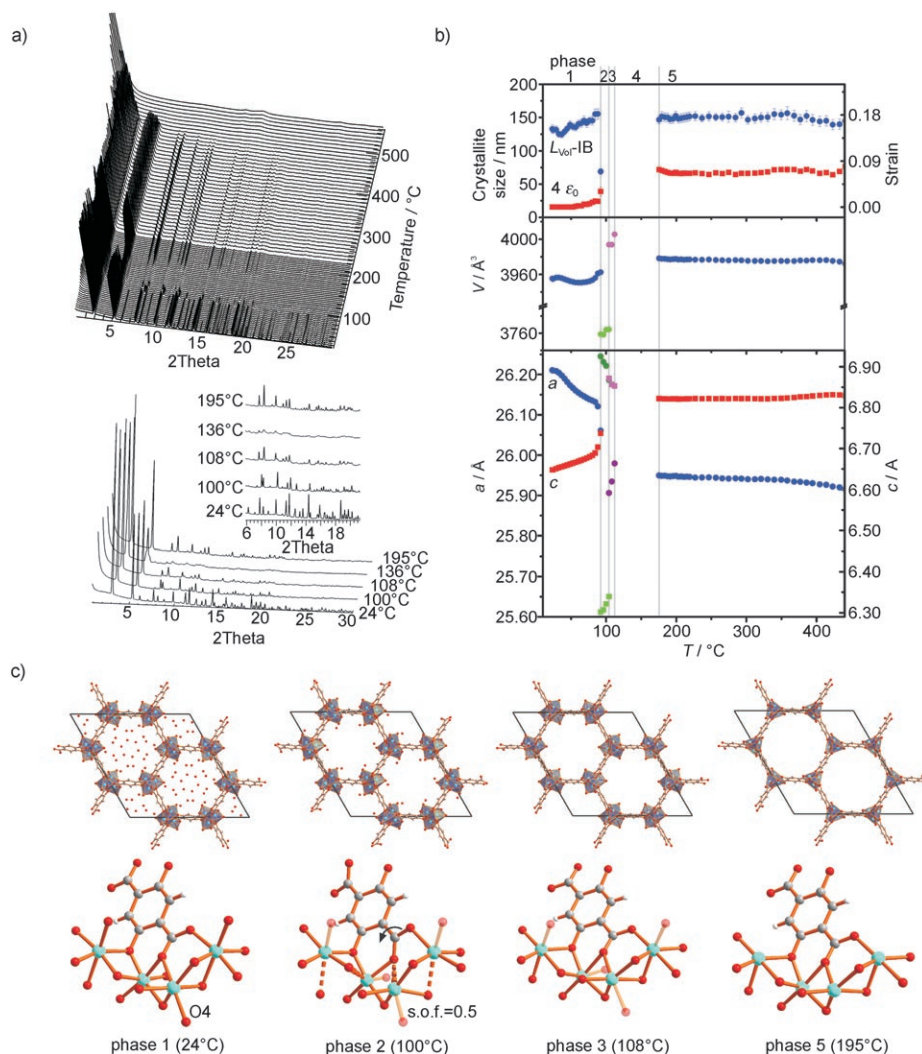


Figure 3. a) Variable-temperature X-ray powder pattern of CPO-27-Zn (top) and selected patterns representing the five different phases which are observed in the experiment (bottom, inset: enlargement of the higher-angle region); b) analysis of lattice parameters, cell volume, and crystallite size and strain; c) Crystal structures of the four sufficiently crystalline patterns showing the successive steps in dehydration (top) and changes in the local molecular environment (bottom). The partial occupancy of the metal-coordinating water molecule is indicated by the level of transparency. The elongated zinc–oxygen distance in phase 2 at 100 °C is indicated by a dashed bond. Also note the increased angle between the planes of the carboxylate group and the phenyl ring in this phase.

(Figure 3c). Most notably, there is an increase in the torsion angle between the plane of the carboxylate group and the phenyl ring, which had slightly decreased from 11.1(1) to 8.2(1)° during dehydration of the first phase and amounts to 26.3(2)° in the structure of phase 2 at 100 °C (Figure 3b). The deflection of the carboxylate oxygen atoms from their previous positions results in a Zn–O distance of the bond in the *anti*-position to the water position, which is elongated by  $\approx 0.2$  Å beyond the already longer than usual distance of it in the previous phase (Table S1 in the Supporting Information), which leaves the zinc atom in a 4+1 or 5+1 coordination depending on the absence or presence of the water molecule in its coordination environment. Also, while all four crystallographically independent water molecules in the

channel are still present at 88 °C (with varying degrees of occupancy), only the one within hydrogen bonding distance to the metal coordinating water remains (with a site occupancy factor of 0.28) at 100 °C. Subsequently, in the third phase at 108 °C, the torsion angle has resided again to a smaller value of 5.9(1)° and shorter Zn–O distance. All of the water molecules in the channel have disappeared by now. The structure of the third phase basically corresponds to the fully dehydrated structure except for the additional presence of the metal-bonded water molecule, which is still approximately half-occupied. The lattice parameters of this phase fit again with the trend encountered for the cobalt compound (e.g. the *a* axis has the approximate value as in the final dehydrated structure and the *c* axis is slightly larger than its value is in the dehydrated state). The third phase is followed by the degradation of the crystallinity as described above until the completely dehydrated structure materializes as the fifth phase. The occurrence of the transitional phase is puzzling considering the similarity between the structure of the third and fifth phase. It must be connected to the removal of the metal-coordinating water molecule. The distinct splitting of the reflections mentioned above points

towards a temporary reduction in symmetry. However, the higher angle reflections of this phase are insufficiently resolved to succeed in indexing. The clearly split low-angle reflections both correspond with lattice planes which are perpendicular to the *ab* plane, the (2 $\bar{1}$ 0) and (300) plane, respectively. Indeed, when the threefold symmetry is removed, yielding space group  $P\bar{1}$ , in which *a* and *b* may differ in value and  $\gamma$  can diverge from 120°, they split into (110), (1 $\bar{2}$ 0), and (2 $\bar{1}$ 0) and (030), (300), and (3 $\bar{3}$ 0), respectively. A profile fit of the low-angle region results in sensible values (Figure S13 in the Supporting Information) of *a*, *b*, and  $\gamma$  which indicates that the hexagonal honeycomb is slightly skewed ( $a = 25.014$ ,  $b = 25.950$  Å;  $\gamma = 116.34^\circ$ ). The remaining unit-cell parameters cannot be derived from the pat-

terns, though. Thus, a definite determination of the structure of CPO-27-Zn in this phase is not possible. In congruence with the more pronounced structural changes occurring in this material, the microstrain in the crystallites of CPO-27-Zn increases significantly during the dehydration process and especially during the reconstructive phase 4 (Figure 3b).

The orientation of the framework in the structurally characterized phases is identical. Consequently, it can be concluded that the dehydration of CPO-27-Zn is a topotactic process in its entirety despite the discontinuities in the evolution of the powder patterns. In light of the above finding, the single-crystal structure at 100 °C must then be considered to be an averaged representation of the structure during its relaxation into the final state which is represented by the structure determination at 150 °C.

## Conclusion

Variable temperature X-ray powder diffraction using synchrotron radiation can be used to obtain structural information of dynamic processes with high time resolution. It thus allows the determination of fast structural changes which are otherwise unavailable. In the present case, it was shown that the dehydration of compound CPO-27-Co progresses in a smoothly topotactic fashion and with no increase in microstrain during the removal of the water. The more strongly bound metal-coordinating water molecule remains at its position until the majority of the bulk water has been removed. Only when this has happened does it start to leave the compound as well. In contrast to its cobalt analogue, CPO-27-Zn passes through several phase transitions upon dehydration. These intricate details of the dehydration mechanism were revealed, and the additional quickly occurring structural changes could be elucidated. The second intermediary phase is a result of a small breathing effect induced by a widening tilt between the planes of the carboxylate group and the phenyl ring. Shortly thereafter, the structure reverts to an arrangement more closely resembling the initial (and final dehydrated) phase. Only very little water remains in the fourth phase, in which the symmetry of the three-fold axis is apparently removed. Once all the water has left the compound, it re-establishes a structure which is analogous to the dehydrated cobalt compound. Investigations of this type promise to greatly enhance our understanding of adsorption and desorption processes.

## Experimental Section

**[Co<sub>2</sub>(dhtp)(H<sub>2</sub>O)<sub>2</sub>·8H<sub>2</sub>O (CPO-27-Co):** 2,5-Dihydroxyterephthalic acid (149 mg, 0.75 × 10<sup>-3</sup> mol) was put into the Teflon inlet and dissolved in THF (10 mL). A solution of cobalt(II) acetate (384 mg, 1.5 × 10<sup>-3</sup> mol) in water (5 mL) was added, the autoclave was sealed and heated at 110 °C for 3 d. The product was isolated by filtration. Yield: 0.204 g (55%). Identity of the bulk phase with a sample for which an elemental analysis was performed<sup>[49]</sup> was established by comparison of the powder X-ray patterns.

**[Zn<sub>2</sub>(dhtp)(H<sub>2</sub>O)<sub>2</sub>·8H<sub>2</sub>O (CPO-27-Zn):** 2,5-Dihydroxyterephthalic acid (0.149 g, 0.75 × 10<sup>-3</sup> mol) was dissolved in THF (10 mL) in a Teflon-lined autoclave of 40 mL volume. Sodium hydroxide solution (3 mL, 1 mol L<sup>-1</sup>) and a solution of [Zn(NO<sub>3</sub>)<sub>2</sub>·6H<sub>2</sub>O (0.446 g, 1.5 × 10<sup>-3</sup> mol) in water (5 mL) were added to this solution while stirring. The autoclave was sealed and heated for three days at 110 °C. The product was collected by filtration as a light-yellow substance which was composed of transparent needles. Yield: 0.309 g (82%); elemental analysis: calcd (%) for C<sub>8</sub>H<sub>22</sub>O<sub>16</sub>Zn<sub>2</sub>: C 19.02, H 4.36, O 50.71, Zn 25.91; found: C 19.83, H 4.03, O 49.11, Zn 25.91.

**Single-crystal structure determination:** Crystallites of CPO-27-Zn obtained by the procedure described above were too small for single-crystal work. The single-crystal structure determinations were, therefore, performed on samples obtained serendipitously in a reaction of zinc sulfate with H<sub>4</sub>dhtp and sodium hydrogencarbonate in a 1:1:2 ratio, which yielded a mixture of CPO-27-Zn and a nonporous coordination polymer with 1:1 zinc to ligand composition. The identity of the single-crystal specimens with the product from the bulk synthesis procedure given above was established by a comparison of observed and calculated powder diffraction patterns by using the results of the bulk synthesis procedure given above.

Intensity data for the hydrated compound CPO-27-Zn and the compound at 100 °C (CPO-27-Zn-373 K) and 150 °C (CPO-27-Z-423 K) were collected on a Bruker D8 diffractometer with a Apex II CCD area detector by using MoK<sub>α</sub> radiation and an Oxford Cryosystems Cryostream Plus device. The data was processed with the SAINT software<sup>[59]</sup> and corrected for absorption with SADABS.<sup>[60]</sup> Structure solution and parameter refinement was performed by using the SHELXTL97 software suite.<sup>[61]</sup> Molecular geometry calculations were performed with PLATON.<sup>[62]</sup> The structures were solved by direct methods, and parameters were refined by using full-matrix least-squares against |F|<sup>2</sup>. All non-hydrogen atoms were refined by allowing for anisotropic displacement.

For the structure determination of CPO-27-Zn, hydrogen atoms were identified from the Fourier difference maps and freely refined. For three of the four water molecules in the channels, the attached hydrogen atoms could not be located. The site-occupation factors of these atoms were set to 1.25 to account for the additional electrons that are contributed by the hydrogen atoms. Also, because the four water molecules in the channel are not well localized (as can be seen from the size of their thermal displacement parameters, Figure S1 in the Supporting Information), their position and thermal displacement factors were fixed in the final refinement run.

For the structure determination of CPO-27-Zn-373 K and CPO-27-Zn-423 K, a crystal was carefully glued on the tip of a glass capillary so that the faces of the hexagonal needle-shaped crystal pertaining to the openings of the honeycomb were not obstructed. The crystal was then placed in a stream of nitrogen gas on the diffractometer and heated with a rate of 10 °C h<sup>-1</sup> consecutively to 100 °C, at which the first data set was collected, and subsequently to 150 °C, at which the second data set was collected.

Crystallographic data are summarized in Table 2. Selected distances and angles for CPO-27-Zn and CPO-27-Co are compared in Table 1.

**Powder X-ray diffraction and thermodiffraction:** Polycrystalline samples of compounds CPO-27-Co and CPO-27-Zn were measured in a capillary on a Siemens D5000 diffractometer by using CuK<sub>α1</sub> radiation. For the variable temperature powder X-ray measurements, a hot-air blower was placed underneath the sample in such a way that the heating zone covered the X-ray beam width. The temperature at the capillary was calibrated by using silver powder as an external standard.

The thermodiffraction experiments were performed in static air or with a flow of nitrogen. A specially modified sample holder was used for the measurements in nitrogen gas which allows a flow of gas to pass through the capillary containing the sample.<sup>[63]</sup> Quartz-glass fibres were placed on both sides of the sample within the capillary to prevent the sample from being blown out of the capillary. Figure S4 (Supporting Information) shows the thermodiffraction patterns of CPO-27-Co and CPO-27-Zn obtained in the home lab.

Table 2. Crystallographic data for the single-crystal structure solution of CPO-27-Zn (room temperature) and CPO-27-Zn-373 K and CPO-27-Zn-423 K.

Compound	CPO-27-Zn	CPO-27-Zn-373 K	CPO-27-Zn-423 K
Formula	C <sub>4</sub> H <sub>11</sub> O <sub>8</sub> Zn	C <sub>4</sub> HO <sub>3</sub> Zn	C <sub>4</sub> HO <sub>3</sub> Zn
<i>M</i> [g mol <sup>-1</sup> ]	252.4	162.42	162.42
<i>T</i> [K]	295	373	423
crystal system	trigonal	trigonal	trigonal
space group	<i>R</i> $\bar{3}$	<i>R</i> $\bar{3}$	<i>R</i> $\bar{3}$
<i>a</i> [Å]	26.259(3)	25.87(4)	25.851(8)
<i>b</i> [Å]	26.259(3)	25.87(4)	25.851(8)
<i>c</i> [Å]	6.6693(15)	6.628(19)	6.706(4)
$\alpha$ [°]	90	90	90
$\beta$ [°]	90	90	90
$\gamma$ [°]	120	120	120
<i>V</i> [Å <sup>3</sup> ]	3982.6(11)	3841(13)	3881(3)
<i>Z</i>	18	18	18
$\rho$ [g cm <sup>-3</sup> ]	1.850	1.264	1.251
$\mu$ [mm <sup>-1</sup> ]	2.79	2.814	2.785
crystal size [mm]	0.12 × 0.02 × 0.02	0.25 × 0.02 × 0.02	0.25 × 0.02 × 0.02
2 $\theta$ range [°]	5.37–54.98	3.14–39.54	3.16–40
no. reflns measured	11 573	3653	5621
no. unique reflns	2032	777	809
<i>R</i> <sub>int</sub>	0.061	0.1668	0.2108
no. observed reflns	1441	385	428
no. parameters/restraints	94/4	73/0	75/0
<i>R</i> <sub>1</sub> [ <i>I</i> > 2 $\sigma$ ( <i>I</i> )]	0.041	0.0698	0.0764
<i>wR</i> <sub>2</sub> (all data)	0.117	0.2495	0.2373
GOF	1.03	1.082	1.023
$\Delta\rho_{\max}/\Delta\rho_{\min}$ [e Å <sup>-1</sup> ]	1.029/–0.586	1.151/–0.775	0.752/–0.818

**Synchrotron diffraction:** Powders of compound CPO-27-Co and CPO-27-Zn were measured at the Swiss-Norwegian Beamlines (BM01A) at ESRF. The samples were filled in 0.5 mm quartz glass capillaries mounted in modified Swagelok fittings and measured under atmospheric pressure from nitrogen with a flow of 1–1.5 mL min<sup>-1</sup>. A hot-air blower was programmed to heat the samples from room temperature to 600 °C with two different heating gradients, 2 °C min<sup>-1</sup> from room temperature to 200 °C and 5 °C min<sup>-1</sup> from 200 to 600 °C. The actual temperature at the capillary was calibrated afterwards by using silver powder as an external

standard. Powder diffraction data were collected during the heating by using a MAR345 area detector and focusing optics. A wavelength of 0.71096 Å, a sample to detector distance of 300 mm with a slit size of 0.3 × 0.3 mm, and an exposure time of 20 seconds was used. This resulted in a time-resolution of 107.2 seconds per pattern (exposure time plus data readout time). The data were converted to normal one-dimensional powder pattern by using the program FIT2D,<sup>[64]</sup> and sigmas were added to the 2 $\theta$ -intensity files with the program add sigma series by Y. Filinchuk.

Rietveld refinements of the patterns were performed by using the WINPOW program.<sup>[65]</sup> All patterns up until complete dehydration, and afterwards every fifth pattern, were refined. Some patterns of CPO-27-Zn during dehydration could not be refined because of insufficient data quality (transitions from phase 1 to phase 2 and from phase 2 to phase 3, all of phase 4). A pseudo-Voigt function over a 2 $\theta$  range from 2.25 to 30.25° was used for the refinements. The patterns were corrected for synchrotron polarization and cylinder absorption. Ten Chebyshev-background parameters were used to describe the background from the capillary and twenty-three distance restraints were used to restrain the distances and angles within the phenyl ring. All the atomic coordinates and the occupancy factors of the water sites were refined. The temperature factors were based on the single-crystal refinement and were refined with one overall temperature factor to minimize the correlation between occupancy and temperature factors. The water positions in the channels were refined as oxygen atoms. Comparison with the single-crystal structure solutions of CPO-27-Co and CPO-27-Zn show that bond lengths obtained from the Rietveld refinements deviate by up to 0.1 Å.

Table 3. Crystallographic data for the Rietveld refinements of CPO-27-Zn and CPO-27-Co.

Compound	CPO-27-Co-297 K	CPO-27-Co-468 K	CPO-27-Zn-297 K	CPO-27-Zn-373 K	CPO-27-Zn-381 K	CPO-27-Zn-468 K
<i>T</i> [K]	297	468	297	373	381	468
space group	<i>R</i> $\bar{3}$	<i>R</i> $\bar{3}$	<i>R</i> $\bar{3}$	<i>R</i> $\bar{3}$	<i>R</i> $\bar{3}$	<i>R</i> $\bar{3}$
<i>Z</i>	18	18	18	18	18	18
<i>a</i> [Å]	26.15786(84)	25.95258(101)	26.20697(85)	26.22054(187)	25.91905(148)	25.94301(132)
<i>b</i> [Å]	26.15786(84)	25.95258(101)	26.20697(85)	26.22054(187)	25.91905(148)	25.94301(132)
<i>c</i> [Å]	6.71822(25)	6.81854(38)	6.64670(23)	6.32019(48)	6.86416(77)	6.81968(56)
<i>V</i> [Å <sup>3</sup> ]	3981.0(2)	3977.3(3)	3953.4(2)	3763.1(5)	3993.5(6)	3975.0(4)
$\lambda$ [Å]	0.710960	0.710960	0.710960	0.710960	0.710960	0.710960
$\rho_{\text{calcd}}$ [g cm <sup>-3</sup> ]	1.797	1.172	1.866	1.384	1.280	1.221
2 $\theta$ range	2.250–30.231	2.248–30.229	2.249–30.230	2.245–30.226	2.246–30.226	2.247–30.228
<i>R</i> <sub>p</sub>	0.0262	0.0264	0.0211	0.0191	0.0171	0.0176
<i>R</i> <sub>wp</sub>	0.0323	0.0297	0.0261	0.0244	0.0181	0.0196
<i>R</i> <sub>exp</sub>	0.0017	0.0016	0.0034	0.0032	0.0044	0.0044
<i>R</i> <sub>Bragg</sub>	1.56	0.81	1.19	0.45	0.41	0.48
no. of reflns	422	414	418	406	415	414
no. of variables	65	45	65	50	51	45
no. of soft distance restraints	23	23	23	23	23	23

Due to the fact that an image plate system was used for data collection, giving imprecise sigmas of the intensities the *R* values may not be straightforwardly applicable for the evaluation of the quality of the refinement on an absolute scale alone. See also the visual representation of the results of the Rietveld refinement in the Supporting Information.

Table 3 contains the crystallographic data for the two representative structures of CPO-27-Co (fully hydrated and dehydrated) and the four well-resolved phases of CPO-27-Zn as an exemplary representation of the results of the Rietveld refinement. Figure S6 to S11 (Supporting Information) contain the corresponding Rietveld plots.

Lattice parameters and size/strain analysis of the thermodiffraction patterns was performed by using TopasP.<sup>[66]</sup> The presentation graphics of the variable temperature powder X-ray diffraction experiment were prepared by using the Powder3D program.<sup>[67]</sup> CCDC 645256–645264 contain the supplementary crystallographic data for this paper. These data can be obtained free of charge from The Cambridge Crystallographic Data Centre via [www.ccdc.cam.ac.uk/data\\_request/cif](http://www.ccdc.cam.ac.uk/data_request/cif).

## Acknowledgements

The skillful assistance from the project team at the Swiss–Norwegian Beamlines, ESRF, and the financial support by the Research Council of Norway through the NANOMAT and KOSK programs (grants 153869/S10 and 165847 V30) are gratefully acknowledged.

- [1] S. L. James, *Chem. Soc. Rev.* **2003**, 32, 276–288.  
 [2] C. Janiak, *Dalton Trans.* **2003**, 2781–2804.  
 [3] S. Kitagawa, R. Kitaura, S. Noro, *Angew. Chem.* **2004**, 116, 2388–2430; *Angew. Chem. Int. Ed.* **2004**, 43, 2334–2375.  
 [4] W. Lin, *J. Solid State Chem.* **2005**, 178, 2486–2490.  
 [5] C. J. Kepert, *Chem. Commun.* **2006**, 695–700.  
 [6] A. K. Cheetham, C. N. R. Rao, R. K. Feller, *Chem. Commun.* **2006**, 4780–4795.  
 [7] S. Kitagawa, S. Noro, T. Nakamura, *Chem. Commun.* **2006**, 701–707.  
 [8] J. L. C. Rowsell, O. M. Yaghi, *Angew. Chem.* **2005**, 117, 4748–4758; *Angew. Chem. Int. Ed.* **2005**, 44, 4670–4679.  
 [9] P. D. C. Dietzel, B. Panella, M. Hirscher, R. Blom, H. Fjellvåg, *Chem. Commun.* **2006**, 959–961.  
 [10] J. L. C. Rowsell, O. M. Yaghi, *J. Am. Chem. Soc.* **2006**, 128, 1304–1315.  
 [11] A. G. Wong-Foy, A. J. Matzger, O. M. Yaghi, *J. Am. Chem. Soc.* **2006**, 128, 3494–3495.  
 [12] M. Dinca, A. Dailly, Y. Liu, C. M. Brown, D. A. Neumann, J. R. Long, *J. Am. Chem. Soc.* **2006**, 128, 16876–16883.  
 [13] H. R. Moon, N. Kobayashi, M. P. Suh, *Inorg. Chem.* **2006**, 45, 8672–8676.  
 [14] Q. Yang, C. Zhong, *J. Phys. Chem. B* **2006**, 110, 655–658.  
 [15] X. Lin, J. Jia, X. Zhao, K. M. Thomas, A. J. Blake, G. S. Walker, N. R. Champness, P. Hubberstey, M. Schröder, *Angew. Chem.* **2006**, 118, 7518–7524; *Angew. Chem. Int. Ed.* **2006**, 45, 7358–7364.  
 [16] M. Dinca, W. S. Han, Y. Liu, A. Dailly, C. M. Brown, J. R. Long, *Angew. Chem.* **2007**, 119, 1441–1444; *Angew. Chem. Int. Ed.* **2007**, 46, 1419–1422.  
 [17] K. Uemura, R. Matsuda, S. Kitagawa, *J. Solid State Chem.* **2005**, 178, 2420–2429.  
 [18] S. Kitagawa, K. Uemura, *Chem. Soc. Rev.* **2005**, 34, 109–119.  
 [19] C. Serre, F. Millange, C. Thouvenot, M. Noguès, G. Marsolier, D. Louer, G. Férey, *J. Am. Chem. Soc.* **2002**, 124, 13519–13526.  
 [20] C. Serre, C. Mellot-Draznieks, S. Surblé, N. Audebrand, Y. Filinchuk, G. Férey, *Science* **2007**, 315, 1828–1831.  
 [21] K. Biradha, M. Fujita, *Angew. Chem.* **2002**, 114, 3542–3545; *Angew. Chem. Int. Ed.* **2002**, 41, 3392–3395.  
 [22] K. Biradha, Y. Hongo, M. Fujita, *Angew. Chem.* **2002**, 114, 3545–3548; *Angew. Chem. Int. Ed.* **2002**, 41, 3395–3398.  
 [23] K. Hanson, N. Calin, D. Bugaris, M. Scancelli, S. C. Sevov, *J. Am. Chem. Soc.* **2004**, 126, 10502–10503.  
 [24] T. K. Maji, G. Mostafa, R. Matsuda, S. Kitagawa, *J. Am. Chem. Soc.* **2005**, 127, 17152–17153.  
 [25] C.-D. Wu, W. Lin, *Angew. Chem.* **2005**, 117, 1994–1997; *Angew. Chem. Int. Ed.* **2005**, 44, 1958–1961.  
 [26] J.-P. Zhang, Y.-Y. Lin, W.-X. Zhang, X.-M. Chen, *J. Am. Chem. Soc.* **2005**, 127, 14162–14163.  
 [27] H. Li, M. Eddaoudi, M. O’Keeffe, O. M. Yaghi, *Nature* **1999**, 402, 276–279.  
 [28] C. J. Kepert, M. J. Rosseinsky, *Chem. Commun.* **1999**, 375–376.  
 [29] K. Biradha, Y. Hongo, M. Fujita, *Angew. Chem.* **2000**, 112, 4001–4003; *Angew. Chem. Int. Ed.* **2000**, 39, 3843–3845.  
 [30] Y.-H. Liu, H.-L. Tsai, Y.-L. Lu, Y.-S. Wen, J.-C. Wang, K.-L. Lu, *Inorg. Chem.* **2001**, 40, 6426–6431.  
 [31] J. Y. Lu, A. M. Babb, *Chem. Commun.* **2002**, 1340–1341.  
 [32] E. J. Cussen, J. B. Claridge, M. J. Rosseinsky, C. J. Kepert, *J. Am. Chem. Soc.* **2002**, 124.  
 [33] M. P. Suh, J. W. Ko, H. J. Choi, *J. Am. Chem. Soc.* **2002**, 124, 10976–10977.  
 [34] B. Rather, M. J. Zaworotko, *Chem. Commun.* **2003**, 830–831.  
 [35] M.-H. Zeng, X.-L. Feng, X.-M. Chen, *Dalton Trans.* **2004**, 2217–2223.  
 [36] Q. Wei, M. Nieuwenhuyzen, F. Meunier, C. Hardacre, S. L. James, *Dalton Trans.* **2004**, 1807–1811.  
 [37] L. Dobrzanska, G. O. Lloyd, H. G. Raubenheimer, L. J. Barbour, *J. Am. Chem. Soc.* **2005**, 127, 13134–13135.  
 [38] E. Y. Lee, S. Y. Jang, M. P. Suh, *J. Am. Chem. Soc.* **2005**, 127, 6374–6381.  
 [39] H. J. Choi, M. P. Suh, *J. Am. Chem. Soc.* **2004**, 126, 15844–15851.  
 [40] E. Y. Lee, M. P. Suh, *Angew. Chem.* **2004**, 116, 2858–2861; *Angew. Chem. Int. Ed.* **2004**, 43, 2798–2801.  
 [41] C.-Y. Su, A. M. Goforth, M. D. Smith, P. J. Pellechia, H.-C. z. Loye, *J. Am. Chem. Soc.* **2004**, 126, 3576–3586.  
 [42] T. K. Maji, K. Uemura, H.-C. Chang, R. Matsuda, S. Kitagawa, *Angew. Chem.* **2004**, 116, 3331–3334; *Angew. Chem. Int. Ed.* **2004**, 43, 3269–3272.  
 [43] G. J. Halder, C. J. Kepert, *J. Am. Chem. Soc.* **2005**, 127, 7891–7900.  
 [44] C.-L. Chen, A. M. Goforth, M. D. Smith, C.-Y. Su, H.-C. z. Loye, *Angew. Chem.* **2005**, 117, 6831–6835; *Angew. Chem. Int. Ed.* **2005**, 44, 6673–6677.  
 [45] M. P. Suh, Y. E. Cheon, E. Y. Lee, *Chem. Eur. J.* **2007**, 13, 4208–4215.  
 [46] J. Jia, X. Lin, A. J. Blake, N. R. Champness, P. Hubberstey, L. Shao, G. Walker, C. Wilson, M. Schröder, *Inorg. Chem.* **2006**, 45, 8838–8840.  
 [47] D. Bradshaw, J. E. Warren, M. J. Rosseinsky, *Science* **2007**, 315, 977–980.  
 [48] B. Chen, M. Eddaoudi, T. M. Reineke, J. W. Kampf, M. O’Keeffe, O. M. Yaghi, *J. Am. Chem. Soc.* **2000**, 122, 11559–11560.  
 [49] P. D. C. Dietzel, Y. Morita, R. Blom, H. Fjellvåg, *Angew. Chem.* **2005**, 117, 6512–6516; *Angew. Chem. Int. Ed.* **2005**, 44, 6354–6358.  
 [50] N. L. Rosi, J. Kim, M. Eddaoudi, B. Chen, M. O’Keeffe, O. M. Yaghi, *J. Am. Chem. Soc.* **2005**, 127, 1504–1518.  
 [51] K. Ståhl, J. Hanson, *J. Appl. Crystallogr.* **1994**, 27, 543–550.  
 [52] G. Artioli, K. Ståhl, J. C. Hanson, *Mater. Sci. Forum* **1996**, 228–231, 369–374.  
 [53] K. Ståhl, G. Artioli, J. C. Hanson, *Phys. Chem. Miner.* **1996**, 23, 328–336.  
 [54] P. Norby, F. I. Poshni, A. F. Gualtieri, J. C. Hanson, C. P. Grey, *J. Phys. Chem. B* **1998**, 102, 839–856.  
 [55] K. Ståhl, J. C. Hanson, *Microporous Mesoporous Mater.* **1999**, 32, 147–158.  
 [56] A. Sani, G. Cruciani, A. F. Gualtieri, *Phys. Chem. Miner.* **2002**, 29, 351–361.  
 [57] G. Cruciani, A. Martucci, C. Meneghini, *Eur. J. Mineral.* **2003**, 15, 257–266.  
 [58] O. Ferro, S. Quartieri, G. Vezzalini, C. Ceriani, E. Fois, A. Gamba, G. Cruciani, *Am. Mineral.* **2004**, 89, 94–101.  
 [59] SAINT: Area-Detector Integration Software., Bruker AXS: Madison, WI, **2004**.  
 [60] SADABS: Area-Detector Absorption Correction, Bruker AXS: Madison, WI, **2004**.



- [61] G. M. Sheldrick, SHELXTL, Program suite for the solution and refinement of crystal structures, Bruker AXS: Madison, WI, **2004**.
- [62] A. L. Spek, *J. Appl. Crystallogr.* **2003**, *36*, 7–13.
- [63] P. Norby, *J. Am. Chem. Soc.* **1997**, *119*, 5215–5221.
- [64] A. P. Hammersley, S. O. Svensson, M. Hanfland, A. N. Fitch, D. Hausermann, *Adv. High Pressure Res.* **1996**, *14*, 235–248.
- [65] K. Ståhl, WINPOW, Version 13-OCT-2006, **2006**.
- [66] TOPAS: General profile and structure analysis software for powder diffraction data, Bruker AXS, Karlsruhe (Germany), **2003**.
- [67] B. Hinrichsen, R. E. Dinnebier, M. Jansen, *Z. Krist. Suppl.* **23** (EPDIC IX proceeding), **2006**, 231–236.

Received: August 30, 2007  
Published online: January 18, 2008